Mon. Not. R. Astron. Soc. **280,** 868–876 (1996)

Variable hydroxyl and methanol masers in G 351.78 – 0.54

G. C. MacLeod★ and M. J. Gaylard

Hartebeesthoek Radio Astronomy Observatory, PO Box 443, Krugersdorp 1740, South Africa

Accepted 1995 December 28. Received 1995 December 18; in original form 1995 October 25

ABSTRACT

The results of monitoring the 1.6-GHz hydroxyl and 6.7-GHz methanol masers in the star-forming region G 351.78 – 0.54 from 1993 to mid-1995 are reported. Variations with time-scales of a few months are superimposed on long-term changes with a time-scale of years in the brightest 1.665- and 1.667-GHz maser peaks and in both 6.7-GHz maser peaks. The methanol maser feature at $+1.2$ km s^{-1} flared at least seven times, varying in brightness from 50 to 300 Jy. Each flare began at the redshifted end of the feature, taking between 10 and 35 d to progress to the blueshifted end. The methanol maser feature at $+1.7$ km s^{-1} experienced smaller changes, the peak flux varying between 150 and 210 Jy. No phase lag was seen across this peak or the 1.665-GHz hydroxyl maser peak at -1.8 km s^{-1} during variations.

Key words: masers – stars: formation – ISM: individual: G 351.78 – 0.54 – ISM: molecules.

1 INTRODUCTION

Variations in interstellar masers have been observed to occur on a wide range of time-scales. In 1.6-GHz hydroxyl masers the range is from less than a day (Clegg & Cordes 1991) through days to years (Sullivan & Kerstholt 1976). The most rapid variations are thought to be due to interstellar scattering, while variations on time-scales longer than a day are probably intrinsic to the masing region.

The most luminous 1.6-GHz OH masers are generally those least likely to vary (Sullivan & Kerstholt 1976). This is understandable if the brightest masers are those most likely to be saturated and so respond linearly to changes, while unsaturated masers would respond exponentially. However, in a few instances observations conflict with this paradigm. The first example of this is the 1.665-GHz OH maser emission at -8.9 km s^{-1} in Cepheus A, which increased in brightness by a factor of 250 over 16 months and became the dominant feature in the spectrum (Cohen & Brebner 1985). The second example is provided by the 1.665-GHz maser peak at -2 km s^{-1} from G 351.78 – 0.54 (Caswell & Haynes 1980), in which the intensity of the left-hand circularly polarized (LCP) component increased by a factor of 6 between 1977 and 1980. At this time it had become the brightest OH maser in the sky. An idea of the subsequent behaviour of this maser can be gained from intermittent observations reported in the literature. Caswell & Haynes (1983) found that it had the same brightness (1000 Jy) on 1980 October 4 and 1981 February 3, and it did not vary by more than 10 per cent between 1980 September and 1981 May (Fix et al. 1982). However, observations by Gosachinskii et al. (1990) on six occasions between 1985 February and 1988 September demonstrated that it was varying markedly again.

The class II methanol masers at 12.2 and 6.7 GHz are closely associated with the interstellar hydroxyl masers. Caswell et al. (1993) found that many 12.2-GHz methanol maser features fluctuated in amplitude by more than 10 per cent on a time-scale of a month. As with hydroxyl masers, the brightest typically show only small changes on time-scales up to years (MacLeod, Gaylard & Kemball 1993). A weak 12.2-GHz methanol maser was found in G 351.78 – 0.54 by MacLeod et al. (1993), and Caswell, Vaile & Ellingsen (1995b) noted that it is variable. In a multi-epoch survey of 6.7-GHz methanol masers, 28 per cent were found to have variable features (Caswell et al. 1995a,b). A twin-peaked 6.7-GHz methanol maser was detected in G 351.78 – 0.54 by Menten (1991). Our observations and those of Caswell et al. (1995a,b) have shown this to be highly variable.

The presence in G 351.78 – 0.54 of bright, strongly varying masers in both hydroxyl and methanol make it a source of particular value, as the possibility of common maser excitation mechanisms and causes of outbursts can be addressed by examining the behaviour of the two maser species and the degree of correlation between the variations in the two

★E-mail: gord@bootes.hartrao.ac.za

masers (Cohen & Brebner 1985). In this case, the varying masers are known to lie within 1 arcsec of each other (Caswell, Vaile & Forster 1995c) and are superimposed on an ultracompact H II region (Fix et al. 1982; Hughes & MacLeod 1993).

We established a monitoring programme for the 1.665- and 1.667-GHz OH masers and 6.7-GHz CH_3OH masers in G 351.78 – 0.54 in order to characterize their temporal behaviour and to search for correlated variations in different transitions and molecular species. In this paper we present the results obtained from three years of monitoring. We investigate the nature of the variations observed in the masers and describe simple models that might explain the results.

2 OBSERVATIONS

Observations were made with the 25.9-m telescope of the Hartebeeshoek Radio Astronomy Observatory. Monitoring was carried out at intervals of 10 to 14 d from 1993 January 29. When it became clear that variations were occurring on shorter time-scales, the monitoring interval was decreased to between 2 and 5 d, from 1993 October 22.

The hydroxyl maser monitoring was carried out in LCP. Additional spectra were obtained occasionally in right-hand circular polarization (RCP). The system temperature at zenith of the 1.6-GHz receiver was 45 K, and the point source sensitivity was 5.3 ± 0.3 Jy K^{-1} in each polarization. The half-power beamwidth at 1.6 GHz was 30 arcmin. A bandwidth of 0.6 MHz was used, giving a velocity range of 28 km s^{-1}. The 256 channels of the correlator provided a resolution of 0.11 km s^{-1}. The integration time per observation was 14 or 21 min, and the resulting 3σ noise level per observation was typically ~ 1 Jy.

The degree of polarization of the 6.7-GHz masers in G 351.78 – 0.54 was measured and found to be less than 3 per cent. The 6.7-GHz feed was linearly polarized, with the E-vector normally oriented in the north–south direction during the monitoring observations, and occasionally in the east–west direction. The half-power beamwidth was 7 arcmin. The system temperature at the zenith was ~ 130 K, and the point source sensitivity was 14.5 ± 0.6 Jy K^{-1}. A bandwidth of 0.32 MHz was used, providing a resolution of 0.056 km s^{-1}. A 3σ noise level of 3–4 Jy was obtained for each observation. To minimize pointing errors and variations in gain, observations were carried out when the source was within 60° of the zenith. Spectra taken at the half-power points of the beam were used to correct pointing errors.

3 RESULTS

3.1 1.6-GHz hydroxyl masers

The general appearance of the OH spectra in LCP and RCP obtained in the monitoring programme is little changed from that seen by Caswell & Haynes (1983). There is a systematic velocity offset of $+0.15$ km s^{-1} in our 1.665-GHz spectra compared to that in Caswell & Haynes (1983) owing to the different line rest frequencies used. Selected 1.665-GHz OH spectra are depicted in Fig. 1. The spectra are divided into three velocity ranges in order that both the strong and weak maser features can be seen clearly and to provide an expanded velocity scale covering the bright, variable feature between -1 and -3 km s^{-1}.

At least four flares were observed in the bright LCP OH maser feature at -1.8 km s^{-1} during the monitoring period, the four flare maxima occurring on 1993 November 19, 1994 June 11, 1994 October 23 and 1995 January 18. Spectra obtained during the rising phase of flare 2 are shown in Fig. 1(a), the falling phase of flare 2 in Fig. 1(b) and during flare 3 in Fig. 1(c). It can be seen in Fig. 1 that while the main OH feature was varying, several of the weaker features also experienced small changes in amplitude.

The RCP 1.665-GHz OH maser feature between -3 and -1 km s^{-1} has also undergone large variations. Caswell & Haynes (1983) quoted a peak flux of 244 Jy for this feature, when the LCP:RCP flux ratio was 3.9:1. We found it to have a peak flux of 173 Jy on 1991 May 22 (LCP:RCP = 4.2:1). Since 1994 August it has been decreasing proportionately across the line profile (Fig. 1d), so that its shape shows little change. The LCP:RCP ratio at -1.8 km s^{-1} remained essentially constant at 2.0:1, but for the peak at -2.2 km s^{-1} it increased from 3.8:1 to 5.8:1. Although the peak at -2.2 km s^{-1} is currently quite prominent, it was essentially undetectable in spectra at both polarizations taken in 1991. By contrast, the OH maser which flared in Cepheus A was almost 100 per cent LCP (Cohen & Brebner 1985).

Fix et al. (1982) showed from VLA observations that the LCP and RCP masers between -3 and -1 km s^{-1} arise within 1 arcsec of each other, and from VLBI observations that the LCP spot size was 40 milliarcsec. At this time the LCP and RCP peaks occurred at slightly different velocities and were interpreted as a Zeeman doublet split by a magnetic field with a strength of 0.3 mG. Inspection of Fig. 1 shows that the main maser feature between -3 and -1 km s^{-1} currently consists of at least two main components at both LCP and RCP. Fits of two Gaussian components to the LCP spectrum of 1994 August 17 and RCP spectrum of August 21 give line centre velocities which differ by less than 0.05 km s^{-1} between the two polarizations. This implies that the magnetic field through both maser spots is now less than 0.1 mG. Similar behaviour was observed in a Zeeman pair in Cepheus A, where the velocity separation decreased over an 11-yr period. This was interpreted as being due to the decay of the magnetic field in the masing region (Cohen, Brebner & Potter 1990).

Maser emission was found in the OH lines at 1.612 and 1.720 GHz, detected by Caswell et al. (1981) and MacLeod et al. (in preparation) respectively. Both are weak and variable, with peak fluxes of a few Jansky.

3.2 6.7-GHz methanol masers

Selected spectra of the 6.7-GHz methanol masers obtained during the rising and falling phases of the four successive flares that occurred after 1993 October 27 are shown in Fig. 2. In contrast to the OH line at -1.8 km s^{-1}, the shape of the $+1.2$ km s^{-1} maser peak shows evidence of changing asymmetrically during the rise and decay of each flare. This feature appears narrow and shifted to more positive velocities during the rising phases (Figs 2a, c and g), and broadened and shifted to more negative velocities when decaying (Figs 2b and d). The asymmetry is much less evident during

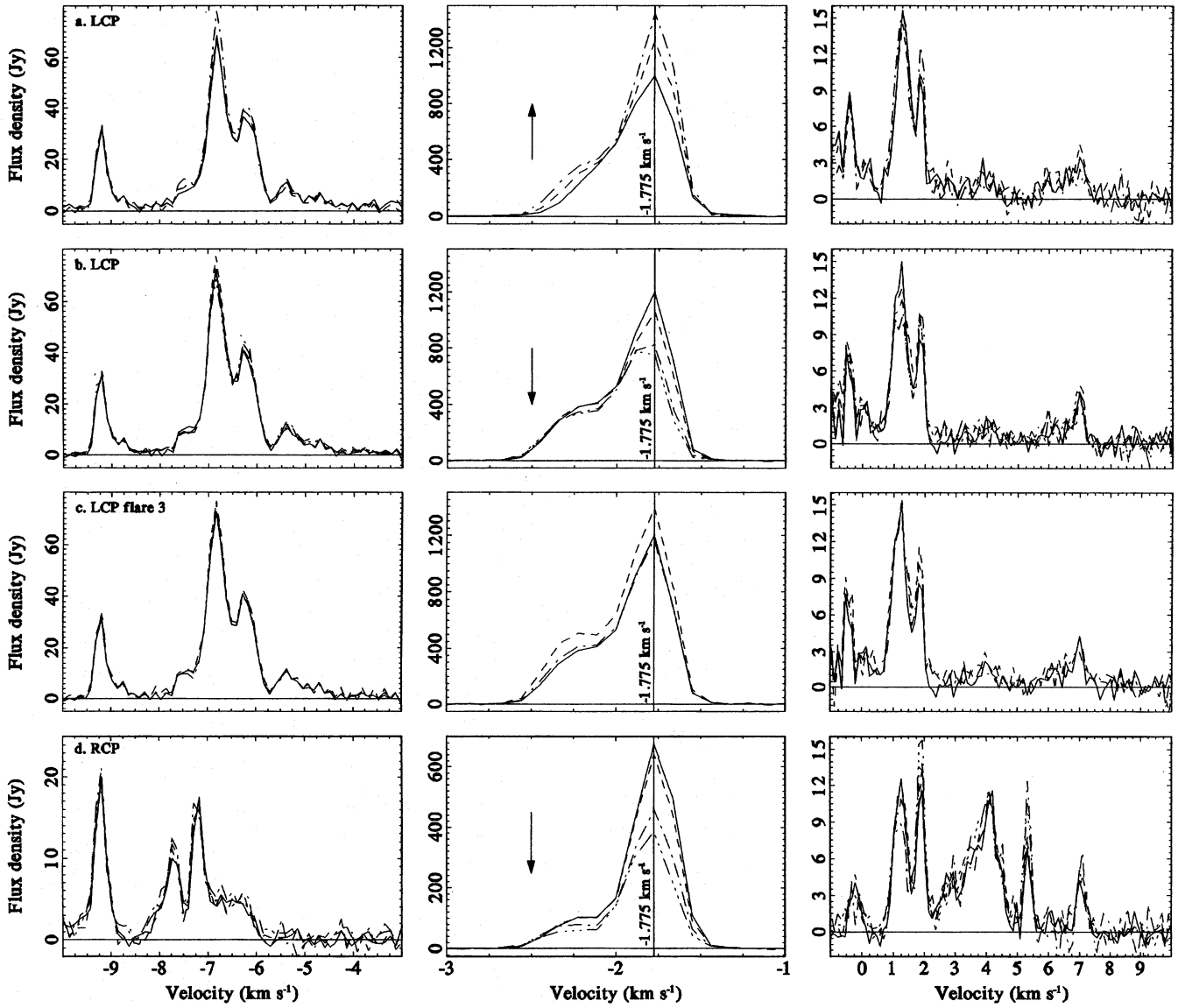

Figure 1. Selected spectra of the 1.665-GHz OH masers. (a) LCP spectra before the maximum of flare 2, (b) LCP spectra after the maximum of flare 2, (c) LCP spectra during flare 3 between 1994 September 18 and November 30, (d) RCP spectra between 1994 August 11 and 1995 June 9. Different line styles are used to illustrate the variations.

flare 5 (Figs 2e and f), possibly because of the small amplitude of the flare. Flare 6 of the $+1.2$ km s^{-1} peak began while the peak was at its lowest level yet recorded (Fig. 2g). It can be seen that the $+1.7$ km s^{-1} feature also brightened during this flare, but uniformly about the line centre. A seventh flare began during the decay of flare 6 and is apparently seen faintly in most of the channels covering the $+1.7$ km s^{-1} peak.

3.3 Maser variation time series

The behaviour of spectral channels covering the main hydroxyl and methanol maser features are shown as time series in Fig. 3. To guide the eye, the right (dashed) vertical line superimposed on Fig. 3 marks the maximum of the well defined OH flare 3, while the left (solid) vertical line marks the peak of the first well-sampled flare in the $+1.2$ km s^{-1} CH_3OH maser feature.

The variations observed in nine velocity channels covering the bright OH emission at 1.665 GHz between -3 and -1 km s^{-1} are shown in Fig. 3(a). Increased scatter in some channels between 1994 November 24 to 1995 August 1 was due to inadequate precision in the Doppler shift correction, which caused slight shifts in the positioning of the emission in the spectrometer band.

Flares of the main OH maser peak are labelled in the -1.775 km s^{-1} channel. Systematic changes in behaviour from one channel to the next can be seen. At the blueshifted end (-2.45 and -2.338 km s^{-1}) the emission increased systematically in brightness from 1993 until the beginning of 1995. Flares 1 and 3 are superimposed on this slow change, but flare 2 is hardly seen. The behaviour of the peak of the

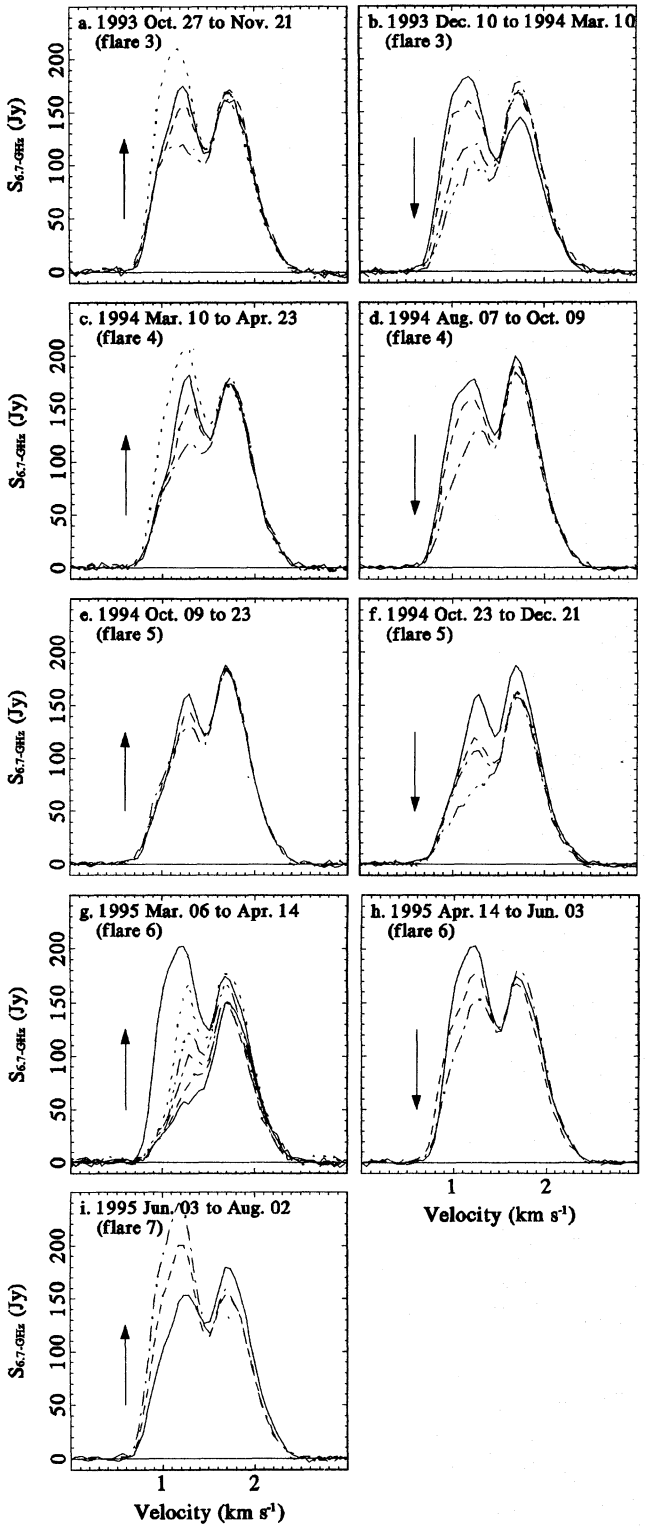

Figure 2. Selected 6.7-GHz methanol maser spectra during five rises (a, c, e, g and i) and four decays (b, d, f and h) of flares 3–7 in the $+1.2$ km s^{-1} peak. The duration of each event is given.

first major component is seen in the channel at -2.225 km s^{-1}; it has declined since flare 3. Flare 2 is much more prominent in the channels between the two peaks. The channels at -1.775 km s^{-1} marks the brighter, right peak, which has declined since flare 2. In the channels on the redshifted edge of this peak, at -1.663 and -1.550 km s^{-1}, there was a sudden dip between flares 1 and 2, followed by a general decay, in contrast to the behaviour of the blue-shifted edge of the emission. The complexity of the behaviour indicates that there are more than two maser components present.

The variations in the other five OH maser peaks brighter than 10 Jy are depicted in Fig. 3(b). Only the emission at -6.8 km s^{-1} changed substantially during the monitoring period. The other four features do vary, but much more slowly.

The behaviour of the three brightest 1.667-GHz OH maser lines at LCP are shown in Fig. 3(c). There was essentially no variation in two of the peaks, but the brightest peak, at -6.945 km s^{-1}, exhibited a slow rise and fall which resembles the long-term behaviour of the 1.665-GHz LCP peaks at -6.838 and -1.775 km s^{-1}.

The peak flux density of the 6.7-GHz methanol masers in G 351.78 – 0.54 was 246 Jy when first detected by Menten (1991), the peak at $+1.2$ km s^{-1} then being the brighter. It was 285 Jy on 1992 January 29 (Norris et al. 1993). We found that it had dropped to 136 Jy on 1992 September 19, but had risen to 309 Jy on 1993 January 29. It is apparent from Fig. 3(d) that the $+1.2$ km s^{-1} feature has undergone at least seven major flares while being monitored. The second methanol maser feature at $+1.7$ km s^{-1} has shown smaller variations during this period, as seen in Fig. 3(e). In Figs 3(d) and (e) only every second velocity channel of the 32 covering the maser profile is shown.

All channels covering the $+1.2$ km s^{-1} methanol peak show similar behaviour, but differences in detail can be seen. For example, flare 4 seems to have been followed by a weak secondary flare which is visible particularly between $+0.785$ and $+1.122$ km s^{-1}. Again, flare 5 is most prominent at $+1.3$ km s^{-1}, but is hardly visible at $+0.8$ km s^{-1}. The channels at $+1.5$ to $+1.6$ km s^{-1} lie between the two peaks at $+1.2$ and $+1.7$ km s^{-1} and show a blend of their behaviour. Three flares are visible in the well-sampled data of the $+1.7$ km s^{-1} peak, and these are labelled in the channel at $+1.684$ km s^{-1}. The first two flares appear to be anticorrelated with the behaviour of the $+1.2$ km s^{-1} peak, while the third occurred at the same time as flare 6 at $+1.2$ km s^{-1}. Flare 3 at $+1.7$ km s^{-1} is complex and may have consisted of two separate events or be confused with flare 6 at $+1.2$ km s^{-1}.

3.4 Phase lags in maser flares

Parameters of flares 3 to 7 in the $+1.2$ km s^{-1} methanol feature, flares 1 and 3 in the $+1.7$ km s^{-1} methanol feature and flare 3 in the -1.8 km s^{-1} hydroxyl feature are presented in Table 1. The methanol maser flares show a consistent pattern of a rapid rise followed by a slow fall lasting two to four times as long, while in the OH maser flares nearly equal time was spent in the rising and falling phases. The duration of each flare was found using the velocity component at the peak of each feature. The flares in the $+1.2$ km s^{-1} methanol feature are aperiodic, the interval between flares ranging from 100 to 200 d.

Examination of the behaviour of the flares in the $+1.2$ km s^{-1} methanol maser peak in Fig. 3(d) shows that there is

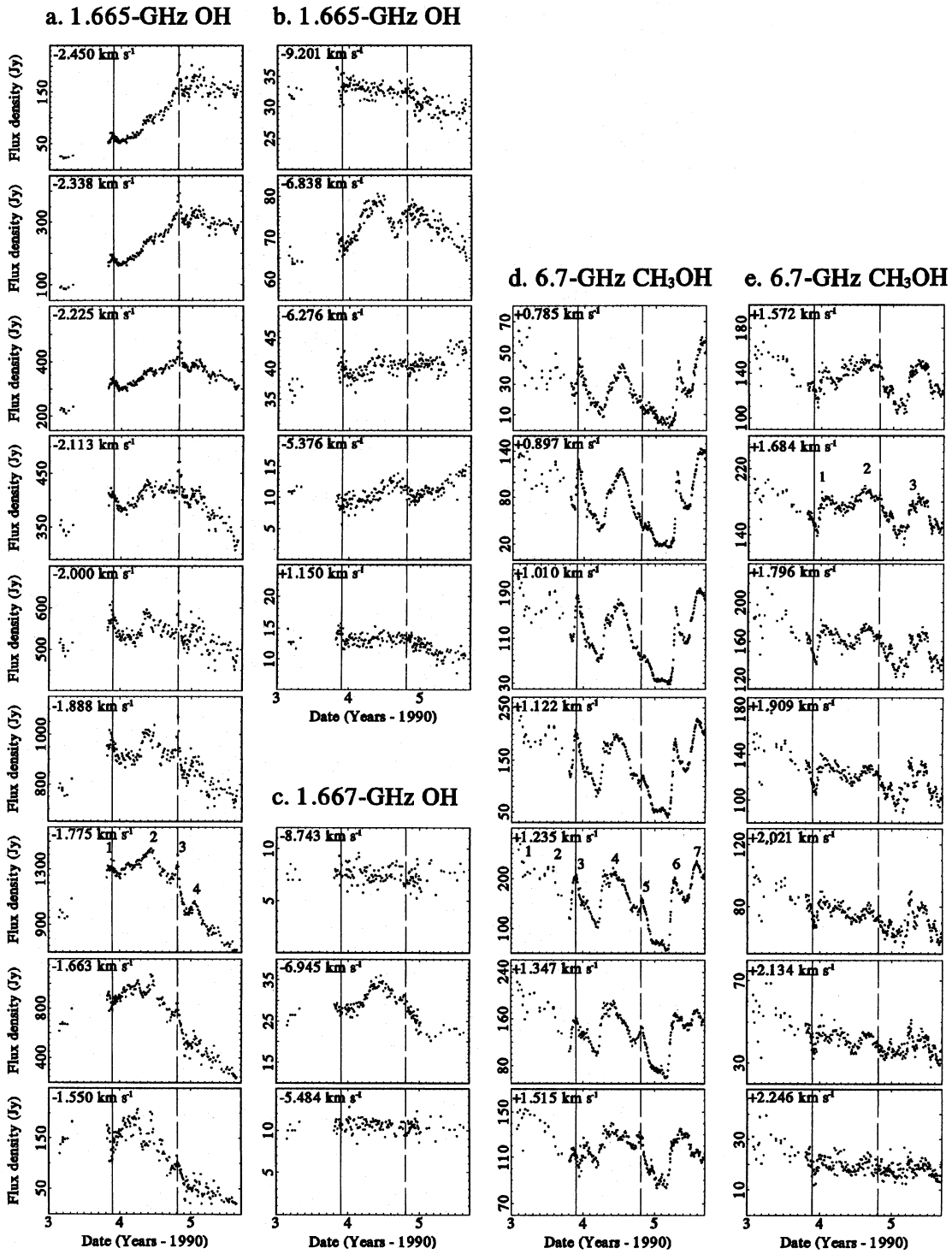

Figure 3. Maser intensities versus time at the given v_{lsr}. (a) -1.8 km s^{-1} 1.665-GHz OH. (b) Other 1.665-GHz OH peaks >10 Jy. (c) Three brightest 1.667-GHz OH lines. (d) $+1.2$ km s^{-1} 6.7-GHz CH_3OH. (e) $+1.7$ km s^{-1} 6.7-GHz CH_3OH. Flares are numbered on the -1.775 km s^{-1} OH, and the $+1.235$ and $+1.684$ km s^{-1} CH_3OH time series.

a tendency for them to occur earlier in the channels at more positive velocities, corresponding to the asymmetric flare development seen in Fig. 2. This behaviour can be regarded as a propagation delay analogous to the phase lag seen in the variations of the 1.612-GHz emission from the front and the back of the OH maser shell of OH/IR stars (Herman & Habing 1985).

An algorithm developed for analysing OH/IR star spectra (West et al. 1992) was used to determine the time delay or phase lag between channels in the spectra during flares of

the 6.7- and 1.665-GHz masers. Cubic splines were fitted through the time series for each channel to provide uniformly spaced, smoothed light curves. The channel with the highest flux was used as the phase reference. The phase lag was estimated by minimizing the sum of squares of the differences between each channel and the reference as a function of time delay. Uncertainties were estimated by randomizing the flux values obtained from the initial fitted spline at each input datum using the error estimate for the datum and then refitting splines through the randomized points. The phase lags of the rising and falling periods of each flare were determined separately.

The phase lags relative to the $+1.235$ km s^{-1} reference channel of the $+1.2$ km s^{-1} methanol feature for the flares that occurred after 1993 October are shown in Fig. 4(a). The phase lag is defined to be positive if the reference channel leads the secondary channel. It is clear that the flares both rise and decay first at the redshifted edge ($\sim +1.4$ km s^{-1}) of the $+1.2$ km s^{-1} feature, and last at the blueshifted edge ($\sim +0.785$ km s^{-1}). Examination of Fig. 4(a) shows that the phase lags are generally linear functions of radial velocity, but change from flare to flare and differ during the rising and falling phase of each flare.

During the decays of flares 4 and 5 the phase lags for the channels at velocities less than $+0.954$ km s^{-1} (Fig. 4a) diverge from linearity; they decrease rather than continuing to increase. These effects are not necessarily real, however. The algorithm used to determine the phase lag between pairs of channels gives reliable results only if both the minimum and maximum of the flare are properly defined in both channels. The decay of flare 4 was interrupted by flare 5; neither minimum is well defined, and we could not obtain a reliable estimate of the phase lag for the rise of flare 5. The second possibility is that the divergence from linearity may be due to the changing profiles of the flares at a function of velocity and time. As noted previously, this applies particularly to flare 5. During flare 7 there is a step increase in the phase lag between the channels at $+0.91$ and $+0.954$ km s^{-1}. If real, this might be caused by a fast flare superimposed on a slower one.

Estimates of the maximum propagation time across the profile for the rise and decay of each flare are given in Table 1. This is defined as the difference in phase lag between the channels at $+0.785$ and $+1.291$ km s^{-1} for flares 1 and 4, and between $+0.954$ and $+1.291$ km s^{-1} for flares 2 and 3. Two values are quoted for flare 7: the first is the difference in phase lag between the channels at $+0.785$ and $+1.291$ km s^{-1}, and the second is the difference between the channels at $+0.954$ and $+1.291$ km s^{-1}.

We were able to obtain estimates of the phase lags for flares 1 and 3 of the $+1.7$ km s^{-1} methanol feature (Fig. 3e). In both cases there is essentially zero phase lag across the profile (Table 1). These phase lag estimates appear in Fig. 4(a) as extensions to more positive velocities of the phase lags of flares 3 and 6 in the $+1.2$ km s^{-1} feature.

Only flare 3 in the -1.8 km s^{-1} OH maser feature (Table 1) occurred across its entire profile (see Fig. 1c). The phase lags across the feature during this flare are less than a day, as depicted in Fig. 4(b). This flare was not observed in the other 1.665-GHz maser peaks (Fig. 2b). Reliable estimates of phase lags could not be obtained for the other OH flares.

4 DISCUSSION

To aid our understanding of the variations of the 6.7-GHz masers, it is useful to estimate the number of components making up each feature. Interferometric observations of appropriate spatial resolution are needed to determine this unambiguously. The only interferometric data available were obtained by Norris et al. (1993) using the Australia Telescope Compact Array, which resolved the $+1.2$ and $+1.7$ km s^{-1} maser peaks into two components each. This is consistent with Gaussian fits to our single-dish spectra, in which two Gaussians leave significant residuals and four are required to leave residuals at the level of the noise. However, the smooth progression of the flares across the $+1.2$ km s^{-1} feature suggests that the number of maser components comprising this feature could be of the same order as the number of spectrometer channels across that part of the spectrum. Otherwise, if several channels covered the same maser component, they would exhibit similar phase lags and a discontinuous progression of the flare across the feature would be expected. The Norris et al. (1993) result does not preclude the possibility that more components are present. Observations of higher angular resolution would be required to test this.

The absence of phase lags in the flares of the -1.8 km s^{-1} 1.665-GHz OH and the $+1.7$ km s^{-1} 6.7-GHz CH_3OH features could be explained by stochastic variations of the component masers or by changes in the pump radiation occurring uniformly behind the masing region. In the case

Table 1. Parameters of flares in the $+1.2$, $+1.7$ km s^{-1} 6.7-GHz CH_3OH and -1.8 km s^{-1} 1.665-GHz OH maser features. The duration of the rising, constant and falling phases are given, together with the propagation times of the rising and falling phases.

molecular species	maser feature (km s^{-1})	flare number	start	maximum	end	rise dur. (d)	prop. time (d)	constant dur. (d)	fall dur. (d)	prop. time (d)
CH_3OH	+1.2	3	1993 Oct 27	1993 Nov 23	1994 Mar 10	27	17	7	100	10
CH_3OH	+1.2	4	1994 Mar 10	1994 Jun 03	1994 Oct 09	38	34	53	85	20
CH_3OH	+1.2	5	1994 Oct 09	1994 Oct 23	1994 Dec 21	14		4	55	20
CH_3OH	+1.2	6	1995 Mar 06	1995 Apr 14	1995 Jun 03	39	24	39	50	
CH_3OH	+1.2	7	1995 Jun 03	1995 Aug 02		60	28/10			
CH_3OH	+1.7	1	1993 Dec 10	1994 Jan 03	1994 Mar 10	24	0 ± 2	29	37	0 ± 2
CH_3OH	+1.7	3	1995 Feb 23	1995 Mar 25		30	0 ± 2			
OH	−1.8	3	1994 Sep 18	1994 Oct 23	1994 Nov 30	35	0 ± 1	0	38	0 ± 1

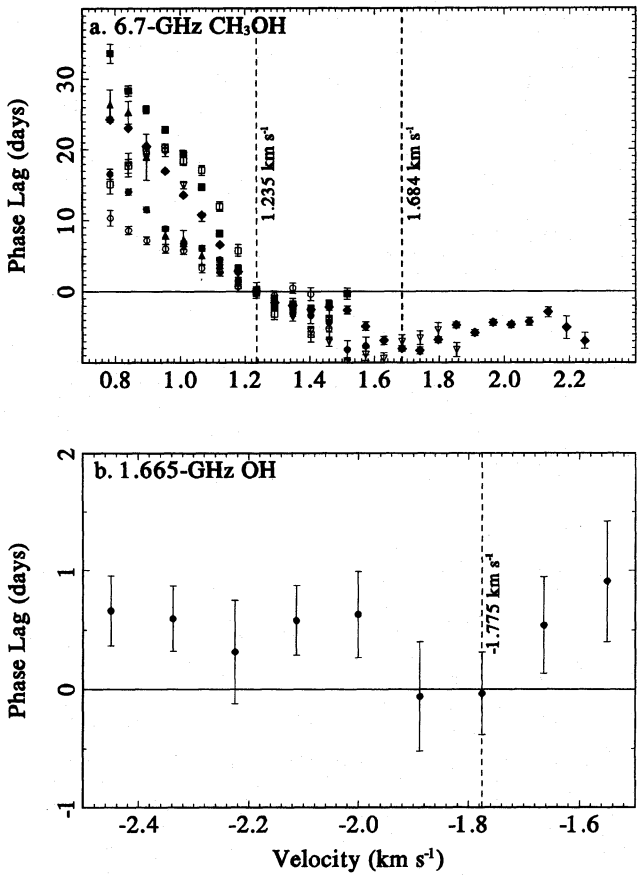

Figure 4. Phase lag versus V_{lsr}. (a) $+1.2$ km s^{-1} CH_3OH: circles: flare 3; squares: flare 4; inverted triangles: flare 5; diamonds: flare 6; triangles: flare 7; solid symbol: rising; open symbol: falling. (b) -1.8 km s^{-1} OH: flare 3.

of the OH flare 3, which was visible across the entire profile of the -1.8 km s^{-1} feature, the latter explanation is more likely. However, it is implausible that the large variations in amplitude and the non-zero phase lags seen in flares of the $+1.2$ km s^{-1} methanol feature could be caused by unrelated stochastic changes in its individual components.

Correlated maser variations would be expected if the variations have a common origin, and indeed both the hydroxyl and methanol masers appear to be associated with the same ultracompact H II region. However, in comparing variations of time series with irregular changes, it is well known that random events produced pseudocorrelations, and a long data span is needed to confirm the reality of apparent correlations.

Thus, comparing the behaviour of the two 6.7-GHz methanol peaks in Fig. 3, while flare 3 at $+1.7$ km s^{-1} is essentially coincident with flare 6 of the $+1.2$ km s^{-1} feature, flares 1 and 2 at $+1.7$ km s^{-1} do not appear to have been related to flares 3, 4 or 5 at $+1.2$ km s^{-1}. Again, comparing the variations in the -1.8 km s^{-1} hydroxyl and $+1.2$ km s^{-1} methanol masers, flares 1, 2 and 3 occurred within 10–20 d of $+1.2$ km s^{-1} CH_3OH flares 3, 4 and 5, yet flare 4 in the -1.8 km s^{-1} OH maser occurred 70 d before the sixth methanol flare. No strong OH flare appears associated with the seventh methanol flare.

Although inspection of Fig. 3 shows that the time-scales of variations of the masers are similar, there is not a one-to-one correspondence between the flares. Therefore it is not clear whether the same process gives rise to the variations in each case. Modelling of the hydroxyl masers suggests that they are pumped by mid-infrared photons originating in warm dust in and around the H II region (Cohen 1989), while the methanol masers are thought to be pumped by photons at millimetre wavelengths arising within the ionized gas (Cragg et al. 1992; Peng & Whiteoak 1992).

One interpretation of the phase lags seen in the $+1.2$ km s^{-1} methanol maser flares is that they represent the projected velocity of physical motion. The magnitude of the projected velocities can be determined from the phase lags if the projected physical size of the methanol masing region is known. Norris et al. (1993) found that the $+1.2$ km s^{-1} maser peak consists of a pair of maser spots separated by 0.02 ± 0.01 arcsec (20 ± 10 au assuming a distance of 1 kpc), located ~ 0.1 arcsec (100 au) from two spots 0.04 arcsec (40 au) apart comprising the $+1.7$ km s^{-1} peak. By comparison, at a distance 1 kpc the physical size of the 1.5-arcsec diameter ultracompact radio source would be 1500 au. The observed phase lags of 10–35 d over 20 au convert to projected velocities of 3500 to 1000 km s^{-1}, assuming that all the maser spots are beamed in the same direction.

Phenomena observed in the flares of the $+1.2$ km s^{-1} methanol maser that require explanation include:

(i) the fast rise and slow decay of the flares;
(ii) the repeatability of the line profile changes from flare to flare;
(iii) the linear progress of the flares across the profile;
(iv) the consistent direction of the progression of flares;
(v) the magnitude of the phase lags;
(vi) the difference in the phase lag from flare to flare;
(vii) the magnitude of the projected velocities inferred from the phase lags, and
(viii) the correlation, or lack of it, with the variations of the other masers.

Changes in the source of pump photons or within the masing gas both provide possible mechanisms. Variable pump sources could include non-thermal radio emission, intermittent ionized jets and dense, ionized stellar winds. Changes in the masing gas could be caused by shocks or disturbances propagating through the masing column. These possibilities are discussed below.

The star-forming region Cepheus A contains radio continuum sources which vary on a time-scale of months, are thought to be non-thermal, and have associated OH masers (Hughes 1991; Hughes, Cohen & Garrington 1995). If this was the cause of the flares in the $+1.2$ km s^{-1} methanol maser feature of G 351.78 – 0.54, then the observed phase lags could be produced by non-uniform changes in the brightness distribution of the emission, such as by variations in brightness propagating behind the masers.

Intermittent, thermal jets have been proposed to account for the multiple epochs of supersonic outflow that are observed in protostars. Velocities observed in these jets are generally hundreds of km s^{-1} (Gouveita Dal Pino & Benz 1994, and references therein), but velocities in the HH 80-81 jet are up to 1400 km s^{-1} (Marti, Rodriquez & Reipurth 1995), which falls within the range apparently required in G 351.78 – 0.54.

If the jet passes at an angle behind the line of masers, the velocity requirements are reduced. Hughes & MacLeod (1993) found that the ultracompact radio source associated with these methanol masers is double, the line joining the components being oriented at nearly right angles to the maser spots comprising the $+1.2$ km s^{-1} feature (Norris et al. 1993). If one component of the double source represents jet ejecta similar to that reported by Marti et al. (1995), and this component was not resolvable when observed by Fix et al. (1982) 2760 d previously, then the double source component separation of 0.74 arcsec (740 au at 1 kpc) implies an ejection velocity of $\sim$500 km s^{-1}. This would represent a lower limit, because the ejection could have occurred at any time between the two sets of continuum observations.

The terminal velocity of winds from naked OB stars is between 1000 and 3500 km s^{-1} (Bieging, Abbott & Churchwell 1989), the stars of earliest type producing the fastest winds. These winds are highly structured and variable (Owocki 1994), and hence could explain aspects of the methanol maser variability. The 6-cm flux density and the size of the emitting region can be estimated if a mass loss rate of $\sim 10^{-5}$ M$_\odot$ yr^{-1}, a wind velocity of $(1–3.5) \times 10^3$ km s^{-1} and an electron temperature of 10^4 K are assumed, these being typical for OB stars (Panagia & Felli 1975). At 1 kpc the corresponding range in flux densities would be $0.5 \leq S_{6\,\mathrm{cm}} \leq 3.3$ mJy, and the range in size of the emitting region would be 30–70 au. These are consistent with the size of the methanol masing regions and the peak flux density in the ultracompact 6-cm source associated with G 351.78 – 0.54 determined by Hughes & MacLeod (1993). However, the ultracompact continuum source has a physical size of $\sim$1500 au at 1 kpc. A difficulty with this model is sustaining high wind velocities if the star is embedded in the H II region within a dense molecular cloud. However, the variability in continuum source 2 of Cep A is thought to be caused by a stellar wind; this source also has associated OH masers (Cohen, Rowland & Blair 1984; Hughes et al. 1995). Panagia & Felli (1975) showed that for a dense, ionized wind the radio flux density is proportional to the wavelength to the power -0.6, making the origin of the emission from the ultracompact source in G 351.78 – 0.54 testable via high angular resolution mapping at wavelengths other than 6 cm.

The second mechanism which might give rise to the observed methanol maser variations and phase lags is that of disturbances within the masing gas. Garay, Moran & Haschick (1989) suggested that the luminous water maser associated with Orion KL could be produced by a magneto-hydrodynamic shock propagating at $\sim$50 km s^{-1} through a dense (10^6 cm^{-3}) magnetic ($\sim$1 mG) molecular gas cloud. The post-shock region would have an overabundance of water, hydroxyl and methanol molecules. A difficulty with this mechanism is the lack of variation in the maser radial velocity during flares, for the water masers in Orion KL vary both in amplitude and velocity (Garay et al. 1989).

The velocities inferred from the phase lags could be explained if the shock fronts arrived at a small angle of incidence to the line of masing components . The clouds that support the methanol masers are believed to have densities of $\sim 10^{4\text{–}5}$ cm^{-3}, above which collisional de-excitation occurs. The sound speed is $\sim$1 km s^{-1}, while the velocities estimated from the phase lags are $>$1000 km s^{-1}. For shock fronts arriving at 10 km s^{-1} the range of angles required to obtain phase lags of 10–35 d is 0°.2–0°.6. At a velocity of 100 km s^{-1} the range of angles is 2°–6°.

The next problem is accounting for the duration of the flares. If the length of the masing gas column is $10^{13\text{–}14}$ cm, then a shock velocity of 10 km s^{-1} would cause each maser component to reach its peak in 100–1000 d. By comparison, the range in time required for the $+1.235$ km s^{-1} peak component to reach a maximum is 15–40 d.

We have insufficient evidence at this time to determine which, if any, of these models could account for all the characteristics of the flares in the methanol and hydroxyl masers, but variations in the maser pumping appears more plausible. Further single-dish monitoring of these masers is needed to define the range of the phase lags in the $+1.2$ km s^{-1} methanol peak, to test the correlations between the variations in different peaks, and to look for evolution in the behaviour of the masers. High-resolution interferometric studies of both the masing transitions and the continuum emission would provide clues to the cause of the phenomena. Simultaneous monitoring of the masing transitions and the centrimetric, millimetric and infrared continuum emission could also shed new light on the maser pumping mechanisms.

5 CONCLUSIONS

The behaviour of the 1.665- and 1.667-GHz OH masers at LCP and 6.7-GHz CH_3OH masers in G 351.78 – 0.54 have been monitored via frequent, high-resolution spectra.

The $+1.2$ km s^{-1} 6.7-GHz methanol maser feature experienced at least seven flares during the monitoring. Each flare begins at the redshifted end of the feature and propagates across the maser profile with time delays in the range 10–35 d. These delays correspond to apparent transverse velocities of greater than 1000 km s^{-1}. The time-scale for variations is 100–200 d. It remains unclear whether variations are correlated with those in the $+1.7$ km s^{-1} methanol peak or the OH maser peaks. Neither the $+1.7$ km s^{-1} methanol peak nor the -1.8 km s^{-1} 1.665-GHz OH maser peak exhibited significant phase lags.

Possible explanations for the variations in the $+1.2$ km s^{-1} methanol peak were examined in terms of changes in the maser pumping or in the masing gas itself; the former appear more likely.

ACKNOWLEDGMENTS

We thank Dr G. D. Nicolson for the generous allocation of observing time. We also thank Dr D. P. Smits for fruitful comments.

REFERENCES

Bieging J. H., Abbott D. C., Churchwell E. B., 1989, ApJ, 340, 518
Caswell J. L., Haynes R. F., 1980, IAU Circ. No. 3509
Caswell J. L., Haynes R. F., 1983, Aust. J. Phys., 36, 361
Caswell J. L., Haynes R. F., Goss W. M., Mebold U., 1981, Aust. J. Phys., 34, 333
Caswell J. L., Gardner F. F., Norris R. P., Wellington K. J., McCutcheon W. H., Peng R. S., 1993, MNRAS, 260, 425

Caswell J. L., Vaile R. A., Ellingsen S. P., Whiteoak J. B., Norris R. P., 1995a, MNRAS, 272, 96
Caswell J. L., Vaile R. A., Ellingsen S. P., 1995b, Proc. Astron. Soc. Aust., 12, 37
Caswell J. L., Vaile R. A., Forster J. R., 1995c, MNRAS, 277, 210
Clegg A. W., Cordes J. M., 1991, ApJ, 374, 150
Cohen R. J., 1989, Rep. Prog. Phys., 52, 881
Cohen R. J., Brebner G. C., 1985, MNRAS, 216, 51P
Cohen R. J., Rowland P. R., Blair M. M., 1984, MNRAS, 210, 425
Cohen R. J., Brebner G. C., Potter M. M., 1990, MNRAS, 246, 3P
Cragg D. M., Johns K. P., Godfrey P. D., Brown R. D., 1992, MNRAS, 259, 203
Fix J. D., Mutel R. L., Gaume R. A., Claussen M. J., 1982, ApJ, 259, 657
Garay G., Moran J. M., Haschick A. D., 1989, ApJ, 338, 244
Gosachinskii I. V., Kandalyan R. A., Nazaretyan F. S., Sanamyan V. A., Yudaeva N. A., 1990, Astrophysics, 33, 302
Gouveita Dal Pino E. M., Benz W., 1994, ApJ, 435, 261
Herman J., Habing H. J., 1985, A&AS, 59, 523
Hughes V. A., 1991, ApJ, 383, 280
Hughes V. A., MacLeod G. C., 1993, AJ, 105, 1495
Hughes V. A., Cohen R. J., Garrington S. T., 1995, MNRAS, 272, 469
MacLeod G. C., Gaylard M. J., Kemball A. J., 1993, MNRAS, 262, 343
Marti J., Rodriquez L. F., Reipurth B., 1995, ApJ, 449, 184
Menten K. M., 1991, ApJ, 380, L75
Norris R. P., Whiteoak J. B., Caswell J. L., Wieringa M. H., Gough R. G., 1993, ApJ, 412, 222
Owocki S. P., 1994, Ap&SS, 221, 3
Panagia N., Felli M., 1975, A&A, 39, 1
Peng R. S., Whiteoak J. B., 1992, in Clegg A. W., Nedoluha G. E., eds, Astrophysical Masers. Springer-Verlag, New York, p. 207
Sullivan W. T. III, Kerstholt J. H., 1976, A&A, 51, 427
West M. E., Gaylard M. J., Combrinck W. L., Cohen R. J., Shepherd M. C., 1992, in Warner B., ed., ASP Conf. Ser. Vol. 30, Variable Stars and Galaxies. Astron. Soc. Pac., San Francisco, p. 277